



HAL
open science

A novel range free visible light positioning algorithm for imaging receivers

Fabián Seguel, Nicolas Krommenacker, Patrick Charpentier, Ismael Soto

► To cite this version:

Fabián Seguel, Nicolas Krommenacker, Patrick Charpentier, Ismael Soto. A novel range free visible light positioning algorithm for imaging receivers. *Optik*, 2019, 195, pp.163028. 10.1016/j.ijleo.2019.163028 . hal-02181111

HAL Id: hal-02181111

<https://hal.science/hal-02181111>

Submitted on 25 Oct 2021

HAL is a multi-disciplinary open access archive for the deposit and dissemination of scientific research documents, whether they are published or not. The documents may come from teaching and research institutions in France or abroad, or from public or private research centers.

L'archive ouverte pluridisciplinaire **HAL**, est destinée au dépôt et à la diffusion de documents scientifiques de niveau recherche, publiés ou non, émanant des établissements d'enseignement et de recherche français ou étrangers, des laboratoires publics ou privés.



Distributed under a Creative Commons Attribution - NonCommercial 4.0 International License

A novel range free visible light positioning algorithm for imaging receivers

Fabian Seguel^{a,b,*}, Nicolas Krommenacker^a, Patrick Charpentier^a, Ismael Soto^b

^a*Université de Lorraine, CRAN CNRS UMR 7039, F-54506 Vandoeuvre-les-nancy, France*

^b*Universidad de Santiago de Chile, Departamento de Ingeniería eléctrica, Avenida Ecuador N° 3519, Estación Central, Chile*

Abstract

In this paper a novel 2-D range free visible light positioning algorithm for imaging receivers is presented. Its performance is obtained by computational simulation. For doing this, an heterogeneous visible light communications network inside a room of dimensions $3 \times 3 \times 3$ meters is modelled in MATLAB. A receiver's height localization interest zone between 1 and 1.5 meters is considered for simulation. Moreover, different field of view angles at the receiver side ranging from 40° to 120° are used in order to measure the behaviour of our proposed algorithm to changes on detector parameters. Optimal detector architecture that, minimizes the error of position estimation is identified and used as case of study. Our method overcomes the traditional convex position estimation (CPE) in terms of accuracy, in all proposed scenarios. The combination of convex polygon positioning (CPP) method and imaging detectors at the receiver side increases the accuracy of position estimation and, robustness to changes in receiver's height. Field of view angles have low impact on method performance when four photodetectors are used. Effect of mismatches in height measurement, tilting and rotation angles are also analysed.

Keywords: Visible light positioning, Range free methods, imaging receivers

*Corresponding author

Email address: fabian.seguelg@usach.cl (Fabian Seguel)

1 Introduction

2 Localization based services have been used massively in the last decade.
3 In particular, the global positioning system (GPS) has been fundamental for
4 the development of various of these services due to its large coverage and low
5 cost. Nevertheless, despite being the most used localization technology in
6 outdoor scenarios, it has not been capable to overcome different issues when
7 facing indoor or dense metropolitan environments. Satellite's line of sight
8 (LOS) signal is blocked in metropolitan areas due to the presence of high
9 buildings and, in indoor scenarios, such as, interior of buildings and tunnels,
10 complete signal loss is experienced since satellite's signals are not capable to
11 penetrate concrete, metal or ground [1].

12 Whilst GPS dominates positioning in outdoor scenarios, different alter-
13 natives have been proposed for indoor environments. Indoor location market
14 is expected to obtain revenues for a value of US\$ 10 billion by 2020 [2]. In
15 order to cover the gap that GPS has left in indoor environments, different
16 technologies have been used as a complement or substitute. Most of the
17 proposals that can be found in literature are based on radio frequency (RF)
18 technology. Mainly, technologies such as Bluetooth, Wi-Fi, RFID and Zigbee
19 [3, 4, 5] are used to provide indoor positioning. Among them, WiFi solutions
20 have been the preferred for domestic implementation since this technology is
21 commonly integrated in off-the-shelf devices and no dedicated infrastructure
22 is required to deliver positioning information [3].

23 In the recent years, visible light communications (VLC) has gained at-
24 tention of researchers due to its capability to provide high data rate wireless
25 communication [6] and high accuracy positioning in indoor environments [7].
26 Moreover, VLC is a cost effective solution since it uses the already deployed
27 lighting infrastructure to provide both, illumination and wireless communi-
28 cation.

29 The advantages of using VLC to provide indoor position systems have
30 encouraged the researchers to propose numerous solutions. VLC based indoor
31 positioning systems (IPS) can be classified in two different groups based on
32 the receiver hardware used for signal detection, i.e, image sensor (IS) based
33 positioning systems and, photo detector (PD) based positioning systems [8].

34 Image sensors provide more useful information related to the LED posi-
35 tion than PD counterpart. In addition to this, different light sources can be
36 directly separated from the image and no multiplexing technique is required
37 [7]. Most of the off-the-shelf devices have already incorporated cameras, mak-

38 ing IS-based positioning easy to implement and inexpensive [9, 10]. The main
39 disadvantage of this type of systems is that IS-based VLC networks have a
40 very limited data rate. Due to this, IS-based networks are not expected to be
41 massively implemented for future wireless networks since they are supposed
42 to deliver high data rates [7]. On the other hand, PD-based VLC systems can
43 provide high data rate communication [8, 11]. Moreover, PDs are inexpensive
44 and easy to install. In order to separate the signal from multiple sources, the
45 usage of multiplexing techniques is required. Depending on the multiplexing
46 technique used to separate the sources, the required hardware for the system
47 can increase in complexity and affect the performance of positioning method
48 as discussed in [12, 13].

49 In general, localization methods can be classified in two types. This clas-
50 sification is based on whether they use distance estimation (range) or some
51 other information to compute mobile node's position [4]. Range based meth-
52 ods estimate the mobile node position by trilateration, multilateration or
53 angulation algorithm. In order to use these algorithms, prior distance esti-
54 mation between transmitter and receivers is required to perform localization.
55 This estimation is derived from signal characteristics, such as, received sig-
56 nal strength, time of propagation or received phase/angle. Receiver signal
57 strength (RSS) simplest method to obtain ranging information. RSS mea-
58 surements are relatively easy to obtain and, most of the devices are built with
59 the required hardware to measure the received signal power level or the re-
60 ceived signal strength indicator (RSSI). In order to estimate the distance from
61 RSS measurements, a precise model of signal propagation is required. Due
62 to this, model precision has high impact in the performance of the algorithm.
63 On the other hand, despite providing a more precise distance estimation than
64 RSS methods, time of propagation and received phase/angle measurements
65 have several drawbacks on its hardware implementation. Time of propagation
66 measurement can be divided in time of arrival (TOA) and time difference of
67 arrival (TDOA) methods. TOA measurements require precise synchroniza-
68 tion of transmitters and receivers which is very difficult to provide. On the
69 other hand, TDOA and phase/angle measurements require synchronization
70 between multiple receivers at the mobile node's side to estimate the distance
71 between transmitter and receiver. In addition to this, due to the high speed
72 of optical signals, receivers must be equipped with a high sampling frequency
73 device in order to perceive the difference in time of arrival.

74 Range based methods have been extensively studied in literature for VLC
75 based IPS. A few number of surveys have been published and the performance

76 in terms of accuracy has been analysed for the most significant methods
77 [7, 9, 14, 13, 10, 15, 16].

78 On the other hand, range free algorithms do not rely in range measure-
79 ments to determine the position of the mobile node. Range free methods use
80 only connectivity information to perform localization. Since different tech-
81 niques such as equalization and coding can be used in order to successfully
82 deliver the message from the anchor node to the mobile user, the effect of
83 signal perturbation does not affect severely the position estimation [17]. In
84 addition to this, no extra hardware is required to measure the signal char-
85 acteristics. Due to this, range free methods can be implemented in any
86 communication standard without special requirements.

87 Range free methods provide a robust positioning compared to range based
88 algorithms [18]. Unfortunately, there exist a trade-off between their high
89 robustness, low hardware requirements and their accuracy. Range free algo-
90 rithms provide coarse-grained localization whilst range based algorithms can
91 provide a fine-grained localization. Traditional range free algorithms used
92 mainly in wireless sensor networks (WSN) have been implemented straight-
93 forward for VLC networks. These algorithms are convex position estimation
94 (CPE) [18] and centroid algorithm [19].

95 In this paper we propose a novel range free localization algorithm for
96 VLC networks that uses imaging detectors and spatial reuse to increase the
97 accuracy. Convex polygon positioning (CPP) algorithm first presented in
98 [20] and formalized in [21, 22] is used to compute the final feasible area of
99 localization. CPP algorithm does not require any signal measurement or
100 synchronization between transmitters and receiver. Due to this, its imple-
101 mentation can be easily done in general purposes devices without powerful
102 hardware capabilities. In this article, the performance of proposed method
103 is analysed. Moreover, the response of algorithm to different perturbations
104 is discussed.

105 The work is organized as follows. In Section 2 the proposed lighting
106 deployment architectures as well as the VLC channel model are presented.
107 In Section 3 the proposed method based on imaging receiver is described.
108 The performance of the method is analysed in Section 4. Finally, the main
109 conclusions of the study and future work will be presented in Section 5.

110 **2 System description**

111 In order to test our method, we assume an homogeneously distributed
 112 lighting deployment as shown in Fig. 1. Since VLC networks use the de-
 113 ployed lighting infrastructure they must provide uniform illumination and
 114 ubiquitous communication coverage. Due to this, LEDs are mostly deployed
 115 as homogeneous networks. Each LED light is separated by the same distance
 116 in the X and Y plane $D_x = D_y = D$.

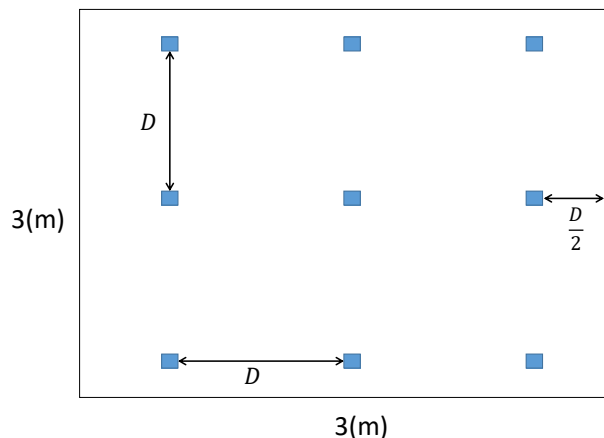


Figure 1: LED deployment for the proposed scenario

117 The received power of the line-of-sight (LOS) signal from each LED light
 118 [23] is expressed as

$$P_i = R_{PD}P_jH_{LOS} + N \quad (1)$$

119 where P_i is the received power by the mobile node i , R_{PD} , P_j and H_{LOS} are
 120 the responsivity of the photo detector, the transmitted power by LED source
 121 j and the channel gain component of line of sight (LOS) link respectively.
 122 The noise N is additive noise modelled as the sum of thermal noise $\sigma_{thermal}$
 123 and shot noise σ_{shot} [24].

124 The LOS channel gain component of the VLC link graphically described
 125 in Fig. 2. The LOS component can be mathematically expressed as [23]

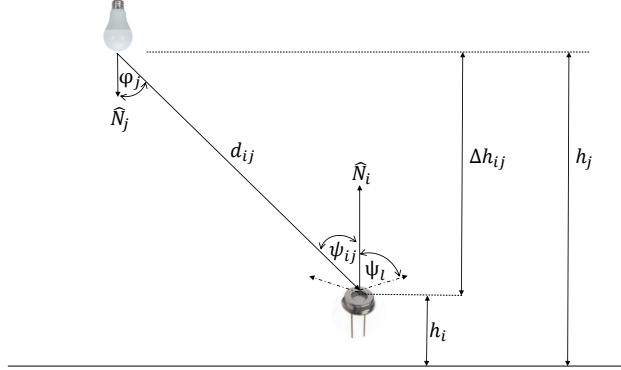


Figure 2: Visible light communications channel model

$$H_{ij} = \begin{cases} \frac{(m_l+1)A}{2\pi d_{ij}^2} \cos^{m_l}(\varphi_{ij}) G(\psi_{ij}) \cos(\psi_{ij}) & 0 \leq \psi_{ij} \leq \Psi_l \\ 0 & \text{elsewhere} \end{cases} \quad (2)$$

126 where m_l is the Lambertian order transmission, A is the effective area of
 127 the PD, d_{ij} is used to denote the distance between transmitter and receiver.
 128 Finally, φ_{ij} and ψ_{ij} are the angle of irradiance and the angle of incidence of
 129 the signal. $G(\psi_{ij}) = T_s(\psi_{ij})g(\psi_{ij})$ is the product of the optical filter gain
 130 and the optical concentrator. The field of view (FOV) of the optical receiver
 131 Ψ_l plays an important role in VLC communications since this parameter
 132 will determine whether the receiver is capable to perceive or not the source
 133 based on the incidence angle ψ_{ij} . The FOV value depends in the quality and
 134 type of the photodiode. From Fig. 2 it can be inferred that the maximum
 135 coverage radius of the LED j , $\max R_j$, depends on the difference height be-
 136 tween transmitter and receiver plane and also receiver FOV. The maximum
 137 coverage radius of the j^{th} LED can be expressed as

$$\max R_j = \tan(\Psi_l) \Delta h_{ij} \quad (3)$$

138 where Δh_{ij} is the difference on the height between the LED and the
 139 mobile node.

140 When a tilt receiver is considered, PD normal vector \hat{N}_i is not oriented
 141 vertically. Due to this, the incidence angle ψ_{ij} and irradiance angle φ_{ij} are

142 not equal, as shown in Fig. 3. In this figure, azimuthal rotation α and
 143 horizontal tilting angle β are displayed.

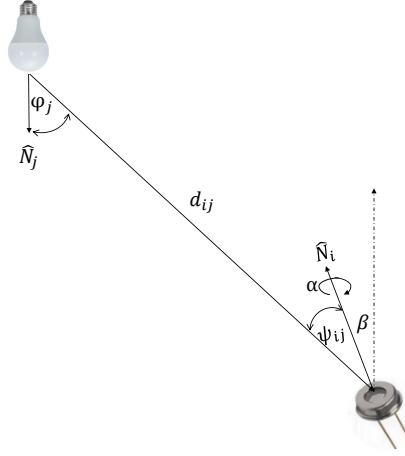


Figure 3: Visible light communications channel model with tilted and rotated receiver

144 When the tilting and rotation angles are considered, incidence angle ψ_{ij}
 145 is affected. Incidence angle depends on azimuthal rotation of the photodetector
 146 α and horizontal PD tilt β . Cosine of the incidence angle used in Eq. (2)
 147 can be re-written as

$$\cos(\psi_{ij}) = \frac{\vec{v}_{PD2LED} \cdot \hat{N}_i}{\|\vec{v}_{PD2LED}\|_2 \|\hat{N}_i\|_2} \quad (4)$$

148 where \vec{v}_{PD2LED} is the vector from PD to the LED source and \hat{N}_i is the nor-
 149 mal vector of the tilt receiver. Magnitude of the vectors are: $\|\vec{v}_{PD2LED}\|_2 =$
 150 d_{ij} and $\|\hat{N}_i\|_2 = 1$. The normal vector of a PD which has been rotated and
 151 tilted in angles α and β respectively can be expressed as

$$\hat{N}_i = \frac{[\sin(\beta) \cos(\alpha), \sin(\beta) \sin(\alpha), \cos(\beta)]}{\|[\sin(\beta) \cos(\alpha), \sin(\beta) \sin(\alpha), \cos(\beta)]\|_2} \quad (5)$$

152 Despite the presence of tilting and rotation angles on the PD, our method
 153 assumes a vertically oriented PD. Due to this, maximum coverage radius
 154 obtained by Eq. (3) is not affected. The final position estimation is expected
 155 to be affected by this mismatch between the real coverage radius of a tilted

156 receiver and its estimated coverage. Effects of the before mentioned mismatch
 157 are discussed in Section 4.

158 Imaging receivers [25] allow multiple-input-multiple-output (MIMO) ca-
 159 pacity for indoor VLC. Imaging receivers consist on the usage of various PDs
 160 at the receiver side. In this work, we consider the usage of imaging detectors
 161 composed by two or four vertically oriented PDs with different FOV angles.
 162 Single PD and imaging receiver architectures are shown in Fig. 4.

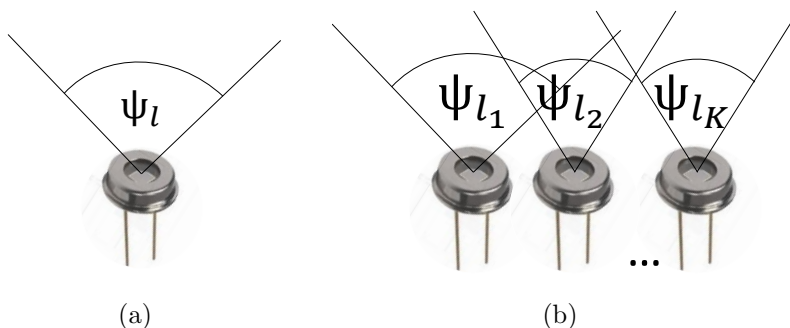


Figure 4: Detector architectures: (a) single photodetector and (b) imaging receiver

163 3 Range free methods for imaging receivers

164 In this section the proposed method is presented. Our method uses the
 165 imaging receivers to reduce the feasible localization area and increase the
 166 accuracy of position estimation.

167 First, in order to compute the maximum radius shown in Eq. (3), previous
 168 knowledge of the mobile node's height is required. Mobile node's height
 169 measurements can be easily obtained by using a low cost range sensor, such
 170 as, ultrasound sensor HC-SR04 [26] or the infrared range sensor VL530lx
 171 [27].

172 The height difference Δh_{ij} is computed as $\Delta h_{ij} = h_j - h_i$ where h_j and h_i
 173 are the height of the j^{th} LED and the i^{th} mobile node respectively. Each VLC
 174 LED light sends a VLC beacon packet periodically. The packet is composed
 175 by the LED ID number, its own coordinates in the three spatial axis and the
 176 coordinates of its closest neighbours. The proposed beacon is shown in Fig.
 177 5.

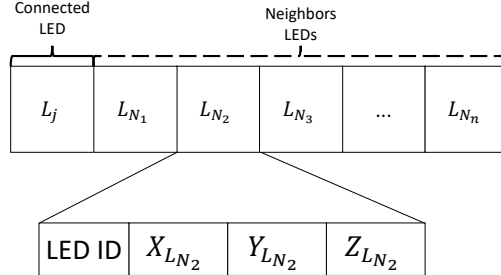


Figure 5: Proposed beacon structure

178 In order to receive information from multiple sources, the algorithm re-
 179 quires the usage of a multiple access technique such as frequency division
 180 multiplexing (FDM), time division multiplexing (TDM), code division mul-
 181 tiplexing (CDM), among others [28, 13].

182 In [29, 28] the performance of TDM, FDM and CDM techniques for indoor
 183 positioning systems using visible LED lights were investigated. As it was
 184 demonstrated, FDM systems obtains better performance in terms of accuracy
 185 when compared with TDM and CDM based localization. Due to this, in our
 186 proposal FDM scheme is used in order to allow each LED transmit their
 187 location information simultaneously.

188 Traditional proximity algorithms use the connectivity information in or-
 189 der to find the area in which the mobile node (MN) could be located. In
 190 particular, convex positioning estimation (CPE) method uses convex opti-
 191 mization to find the minimum bounding rectangle of the feasible connection-
 192 based set [30]. This feasible localization area is a convex set in \mathbb{R}^2 [31].

193 These type of algorithms assume a fixed coverage radius R_j . As detailed
 194 in Section 2, the maximum coverage area strongly depends on detector's FOV
 195 and height difference (see Eq. (3)).

196 In Fig. 6 intersection patterns of maximum coverage area of each VLC
 197 source are displayed for single PD detector and imaging receiver composed
 198 by 2 PDs.

199 As it can be seen, the usage of two PDs with different FOV angles creates
 200 a more dense intersection pattern. Due to this, the complete area of the
 201 considered room is divided into smaller feasible regions.

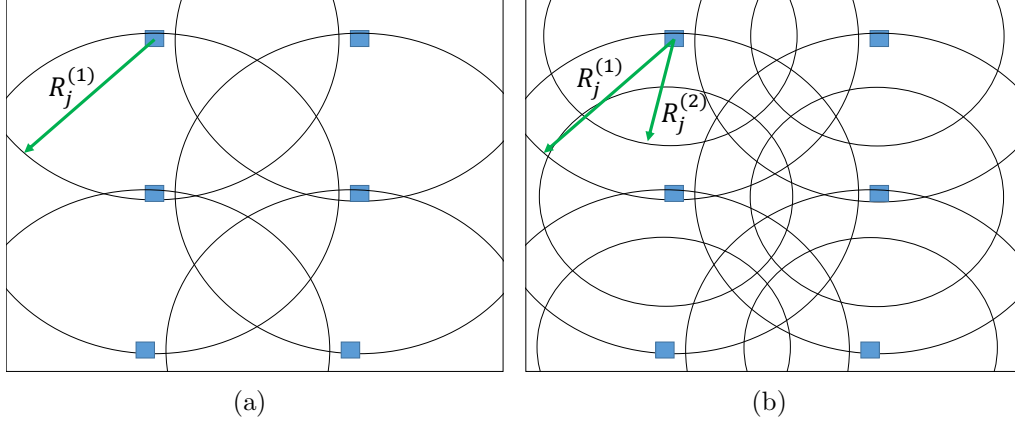


Figure 6: Intersection pattern of feasible localization area based on (a) single PD and (b) imaging receiver

202 Since imaging receivers are used in our method, the constraints of original
 203 CPE algorithm proposed in [30] have been modified in order to take into
 204 account multiple detectors as detailed in Eq. (6)

$$\begin{aligned}
 & \underset{\mathbf{x} \in \mathbb{R}^2}{\text{minimize}} && \mathbf{D}^T \mathbf{x} \\
 & \text{subject to} && \|\mathbf{x} - \mathbf{C}_1\|_2 \leq R_1^{(1)}, \\
 & && \|\mathbf{x} - \mathbf{C}_1\|_2 \leq R_1^{(2)}, \\
 & && \dots, \\
 & && \|\mathbf{x} - \mathbf{C}_1\|_2 \leq R_1^{(K)}, \\
 & && \|\mathbf{x} - \mathbf{C}_2\|_2 \leq R_2^{(1)}, \\
 & && \|\mathbf{x} - \mathbf{C}_2\|_2 \leq R_2^{(2)}, \\
 & && \dots, \\
 & && \|\mathbf{x} - \mathbf{C}_j\|_2 \leq R_j^{(K)}
 \end{aligned} \tag{6}$$

205 where \mathbf{D} is a two dimensional vector which takes the values $\mathbf{D} = [1 \ 0]$, $\mathbf{D} =$
 206 $[-1 \ 0]$, $\mathbf{D} = [0 \ 1]$ and $\mathbf{D} = [0 \ -1]$ in order to find the minimum and maxi-
 207 mum of the feasible localization area for both axis. Position of the connected
 208 cell in X and Y axis, \mathbf{C}_j , and maximum coverage radius of connected cells for
 209 each detector $R_j^{(k)}$ are considered as constraints of the optimization problem.
 210 Number of constraints in the optimization problem is directly related to the

211 number of PDs (K) at the receiver side and the number of connected cells.

212 Once the connectivity localization area is found, the neighbour LED in-
 213 formation is used in order to reduce the feasible localization region. A two
 214 steps algorithm is used to find the overlapped neighbours and convert the
 215 feasible rectangle into a minimum convex polygon.

216 First, overlapped cells to the bounding box are found by solving the
 217 convex optimization problem shown in Eq. (7)

$$\begin{aligned}
 & \underset{\mathbf{x} \in \mathbb{R}^2}{\text{minimize}} && \|\mathbf{x} - \mathbf{C}_m\|_2 - R_m^{(k)} \\
 & \text{subject to} && \mathbf{x} \preceq \mathbf{x}_{max}, \\
 & && -\mathbf{x} \preceq -\mathbf{x}_{min}
 \end{aligned} \tag{7}$$

218 where \mathbf{x}_{min} and $\mathbf{x}_{max} \in \mathbb{R}^2$ are the minimum and maximum values of the
 219 feasible connectivity localization area, \preceq is an element-wise comparator, \mathbf{C}_m
 220 is the position of the non-connected neighbour cell m and $R_m^{(k)}$ is its maxi-
 221 mum coverage radius for each detector $k = \{1, 2, \dots, K\}$. In this work the
 222 maximum number of detectors K takes the values $K = \{2, 4\}$. If the solution
 223 of minimization problem in Eq. (7) is less or equal to zero, the neighbour
 224 LED is considered to be overlapped with the connectivity localization area.
 225 A binary connectivity indicator is used to determine whether the neighbour
 226 is overlapped or not is proposed in Eq. (8).

$$\text{Overlapping} = \begin{cases} 1 & \text{if Eq.(7)} < 0 \\ 0 & \text{if Eq.(7)} \geq 0 \end{cases} \tag{8}$$

227 Once the overlapped cells are found, intersection points between the con-
 228 nectivity localization area and overlapped cells are computed. Using these in-
 229 tersection points, the feasible localization zone is reduced to a convex polygon
 230 that takes into account the overlapped non-connected cells. Both methods,
 231 CPE and CPP, use the imaging properties on the receiver side to minimize
 232 the feasible localization area. In particular, CPE estimates the mobile device
 233 position based on the solution of Eq. (6) as follows

$$(\hat{x}_{MN}, \hat{y}_{MN}) = \left(\frac{x_{min}^* + x_{max}^*}{2}, \frac{y_{min}^* + y_{max}^*}{2} \right) \tag{9}$$

234 where x_{min}^* and y_{min}^* are the minima of feasible area in X and Y axis
 235 respectively. Similarly, x_{max}^* and y_{max}^* are the maxima of feasible area in X
 236 and Y axis respectively.

237 The proposed method CPP estimates the mobile node position as the
 238 centroid of the feasible localization area. Since the final feasible localization
 239 area of CPP is a convex close polygon in \mathbb{R}^2 , its centroid can be obtained by

$$\begin{aligned}\hat{x}_{MN} &= \left(\frac{1}{6A_p} \sum_{j=1}^P (x_j + x_{j+1})(x_j y_{j+1} - x_{j+1} x_j) \right) \\ \hat{y}_{MN} &= \left(\frac{1}{6A_p} \sum_{j=1}^P (y_j + y_{j+1})(x_j y_{j+1} - x_{j+1} x_j) \right)\end{aligned}\quad (10)$$

240 where P is the total number of vertices of the convex polygon, (x_j, y_j)
 241 are the components in the X and Y axis of each point in the set and A_p is
 242 the area of a convex polygon computed as

$$A_p = \frac{1}{2} \sum_{j=1}^P (x_j y_{j+1} - x_{j+1} y_j) \quad (11)$$

243 To solve problem convex optimization problems (6) and (7) we used CVX,
 244 a package for specifying and solving convex programs in MATLAB [32].

245 4 Numerical results

246 The LED deployment shown in Fig. 1 is used to evaluate the performance
 247 of our proposed algorithm. Parameters used for simulation are delivered in
 248 Table 1. Four different receiver architectures are proposed and detailed in the
 249 table below, these are, PD(a), PD(b), PD(c) and PD(d). These architectures
 250 are used in order to measure the effect of using different FOV combinations
 251 at the receiver side. Our proposed method is compared with CPE algorithm.
 252 Numerical results where obtained using a square testing grid with separation
 253 of 0.1 meters between each testing point. Two different receiver heights are
 254 proposed in order to measure the impact of Δh_{ij} on algorithm performance.
 255 In addition to this, for measuring the impact of tilting and rotation at the
 256 receiver side, an horizontal tilting angle β is assumed to be in the range of
 257 $\pm 2^\circ$ and rotation angle $\alpha \in [0^\circ, 360^\circ]$.

258 4.1 Impact of receiver architecture and height

259 In this section the impact of changes in receiver architecture and height
 260 are analysed. Different combinations of FOV angles provide different inter-
 261 section patterns (see Fig. 6). Due to this, measuring the effect of multiple

Parameter	Value	Parameter	Value
$\Phi/2$	70°	m_l	0.6461
P_j	10W	A	10^{-4} m^2
T_s	1	Simulation grid	$0.1 \times 0.1 \text{ m}$
Room size	$3 \times 3 \times 3 \text{ m}$	Number of LEDs	9
Δh_{max}	2 m	Δh_{min}	1.5 m
ρ	0.8	Mismatch	$\pm 0.04 \text{ m}$
FOV PD(a)	60 and 80°	FOV PD(b)	60 and 100°
FOV PD(c)	40, 60, 80 and 100°	FOV PD (d)	60, 80, 100 and 120°
$ \beta_{tilt1} $	1°	$ \beta_{tilt2} $	2°
α_{rot1}	0°	α_{rot2}	90°
α_{rot3}	180°	α_{rot4}	270°

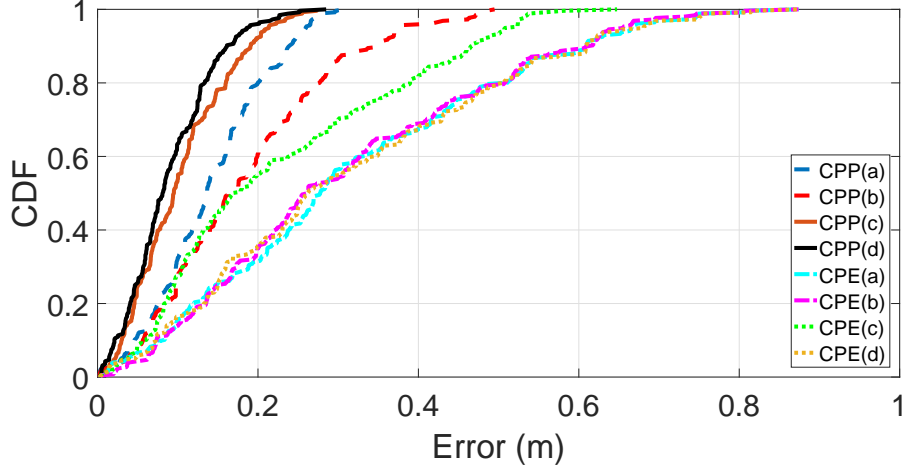
Table 1: Parameters for computational simulation

coverage radius $R_j^{(k)}$ is important. Four different FOV combinations detailed in Table 1 are proposed. In Fig. 7 the cumulative distribution function (CDF) of errors is displayed for $\Delta h_{ij} = 1.5$ meters and $\Delta h_{ij} = 2$ meters using the proposed detector architectures. The acronym of the algorithm along with the receiver architecture is used as abbreviation to simplify the performance analysis. For instance, CPP(a) stands for the performance of CPP algorithm using the receiver architecture PD(a) of Table 1.

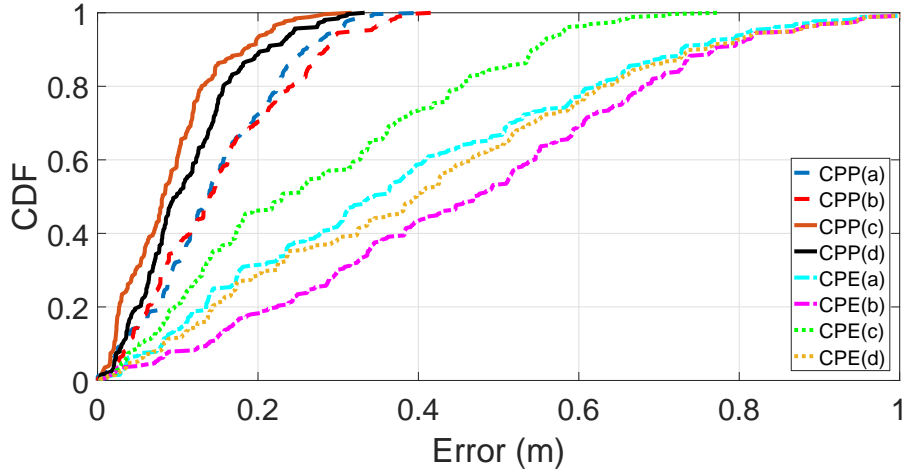
As it can be seen, the combination of CPP method and imaging receiver overcomes imaging receivers based CPE. The best performance is achieved when a detector composed by four PDs is used at the receiver side. Changes in receiver's height have small impact on CPP performance when multiple receivers are used. CPP method shows to be more robust to changes on the FOV combination compared to CPE algorithms. Small changes on FOV combination used at the receiver can severely affect the CPE method performance. For instance, when using four PDs at the receiver side, the error of CPE(d) is far larger than CPE(c). On the contrary, CPP performance is similar for PD(c) and PD(d) architectures in both proposed scenarios.

In Table 2 the best cases for each detector architecture are compared.

As the receiver height difference increases to from $\Delta h_{ij} = 1.5(m)$ to $\Delta h_{ij} = 2(m)$, mean accuracy of CPP method changes. From Table 2 it can be seen that the best architecture for $\Delta h_{ij} = 1.5(m)$ is PD(c). The overall performance of PD(c) architecture overcomes PD(d), which shows to be more sensitive to changes in receiver's height.



(a)



(b)

Figure 7: Performance of imaging receiver based convex polygon positioning (CPP) and convex position estimation (CPE) for (a) $\Delta h_{ij} = 1.5$ (m) and (b) $\Delta h_{ij} = 2$ (m)

285 4.2 Impact of mismatch receiver's height measurements

286 In order to estimate the maximum coverage radius, CPP method requires
 287 previous knowledge of receiver height. Since ranging information is not al-
 288 ways precise, the algorithm will be affected by the mismatch between real
 289 height and measured height. In Fig. 8 (a) real measurements of receiver

Δh_{ij} (m)	Parameter	CPP(a)	CPP(b)	CPP(c)	CPP(d)
1.5	Mean(m)	0.1399	0.1840	0.1030	0.0899
1.5	σ_{error} (m)	0.0697	0.1104	0.0606	0.0548
2	Mean(m)	0.1457	0.1518	0.0906	0.1119
2	σ_{error} (m)	0.0839	0.0941	0.0624	0.0695

Table 2: Performance in terms of mean error and standard deviation of the best PD architectures

290 difference height performed by an ultrasonic sensor (HC-SR04) for $\Delta h_{ij} = 2$
 291 meters are shown. As it can be seen, measurements done by the sensor are
 292 not perfect. In addition to this, outliers are present. In order to overcome
 293 this problem, a median filter is commonly use for outlier elimination.

294 In Fig. 8 (b) the filtered measurements of Δh_{ij} are displayed. As it can be
 295 seen, outliers are eliminated from signal. Moreover, errors in the difference
 296 height measurement smaller than 4 centimetres are obtained.

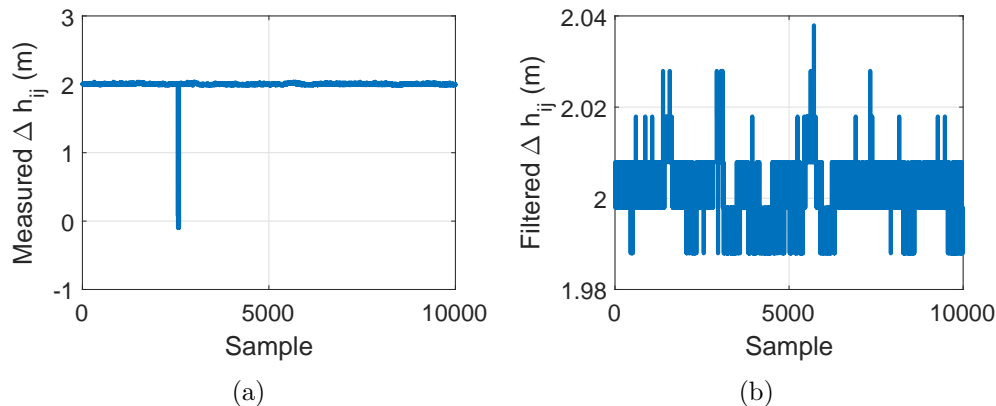


Figure 8: Difference height distance measurements (a) raw measurements and (b) filtered measurements

297 The standard deviation of the filtered difference height measurement
 298 $\sigma_{\Delta h_{ij}} = 0.0064$ (m). In Fig. 9 the effect of mismatch measurements of
 299 receiver's height is shown. The performance of the method to mismatch
 300 estimations in an interval between ± 4 centimetres is simulated. This inter-
 301 val is proposed based on the measurements obtained in Fig. 8 (b). CPP
 302 method using PD(c) architecture at receiver side is used to analyse the effect
 303 of mismatch measurements.

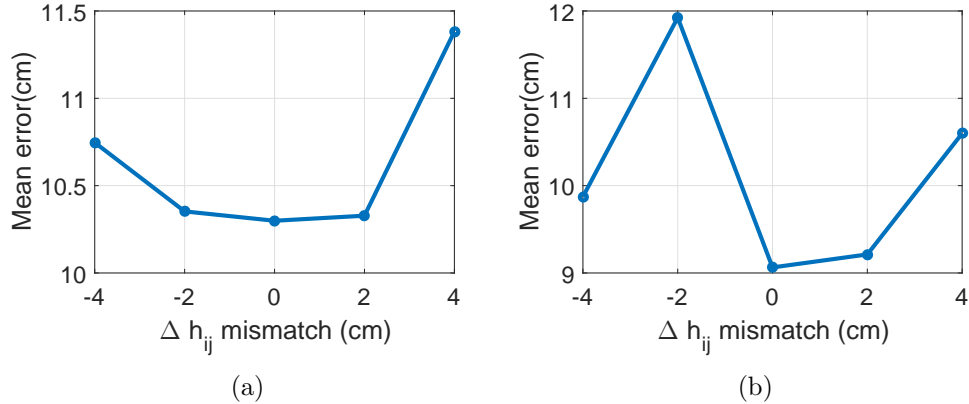


Figure 9: Impact of mismatch measurements on receiver's height using PD(c) architecture for (a) $\Delta h_{ij} = 1.5$ meters and (b) $\Delta h_{ij} = 2$ meters

304 As it can be seen in Fig. 9, the impact of a mismatch in the estimation
 305 of height difference in the range of ± 4 centimetres increases the mean error
 306 in less than 1 centimetres when PD(c) architecture is used, for a height
 307 difference $\Delta h_{ij} = 1.5$ meters. In addition to this, negative mismatch produces
 308 lower error than positive mismatch.

309 On the other hand, for $\Delta h_{ij} = 2$ meters, mismatches in measurement
 310 have higher impact, increasing the mean error from less than 10 centimetres
 311 to approximately 12 centimetres as shown in Fig. 9 (b). The impact of
 312 mismatch measurements on method performance increases along with the
 313 difference height between the source and receiver.

314 4.3 Impact of tilting and rotation angles

315 In order to perform localization, CPP method uses an initial estimation of
 316 the maximum coverage radius based on the FOV of receiver. Since receivers
 317 and transmitter are not always parallel, the maximum coverage range may
 318 vary based on the tilting angle of the receiver. In Fig. 10 the effect of
 319 tilting and rotation angles on method performance are shown. Mean error of
 320 the algorithm is obtained by computational simulation for tilting angles of
 321 $\beta = 1^\circ$ and $\beta = 2^\circ$ as proposed in Table 1. Furthermore, four discrete values
 322 of rotation angle α are analysed.

323 As it can be seen the rotation angle α has low impact in method per-
 324 formance for a difference height $\Delta h_{ij} = 1.5$ meters. On the other hand, as
 325 tilting angle β increases, accuracy of the proposed method decreases. The

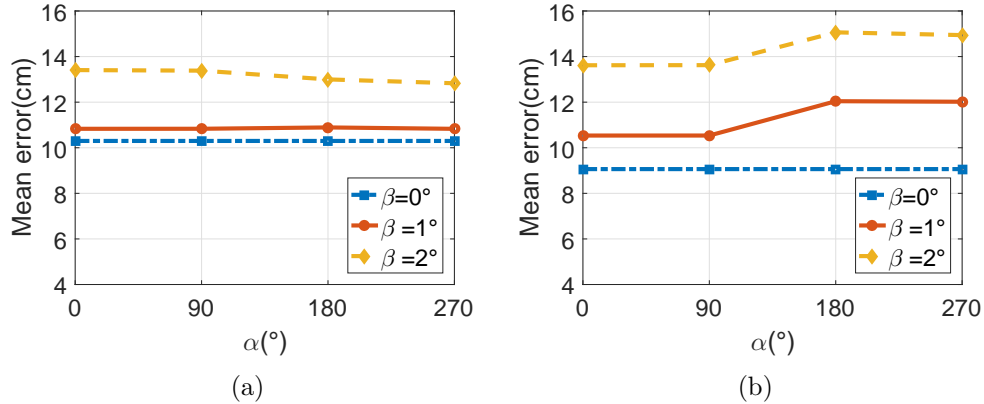


Figure 10: Impact of tilting and rotation angles using PD(c) architecture for (a) $\Delta h_{ij} = 1.5$ meters and (b) $\Delta h_{ij} = 2$ meters

326 impact of tilting angle β in CPP accuracy is stronger when $\Delta h_{ij} = 2$ meters.
 327 In addition to this, rotation angles between 180° and 270° also significantly
 328 increase the error in this scenario.

329 5 Conclusions

330 In this paper a novel range free method that uses imaging receivers to
 331 increase the accuracy is presented. The proposed method, convex polygon
 332 positioning, uses the knowledge of lighting deployment and FOV angle diver-
 333 sity to estimate the mobile node position. Since the method uses diversity
 334 at the receiver side, the algorithm is capable to increase the performance
 335 without increasing the number of access points (LED lights) deployed.

336 The proposed algorithm shows to be more accurate than CPE method.
 337 CPP has shown to be robust to changes in receiver's height. Small variations
 338 on the position estimation error are produced when changes in receiver's
 339 height occur.

340 Results show that a larger number of photodetectors used at the receiver
 341 side can increase the accuracy of CPP method as well as its robustness. The
 342 best accuracy and robustness are obtained when a total of $K = 4$ PDs are
 343 used.

344 The effect of mismatch measurement of receiver height are also analysed
 345 in this article. Errors up to 4 centimetres in the height estimation may
 346 increase the mean error of proposed method as far as 3 (cm).

347 In addition to mismatch height measurements, response to tilting and
348 rotation angles is discussed. It has been shown that tilting and rotation
349 angles affect more significantly the proposed method when the difference
350 height $\Delta h_{ij} = 2(\text{m})$. Mean error shows to be more sensitive to tilting angle
351 β than rotation angle α for a $\Delta h_{ij} = 1.5(\text{m})$.

352 For future work, an optimized imaging receiver for range free localization
353 will be implemented in order to test the procedure in real scenarios. More-
354 over, different LED placement configuration will be tested in order to find
355 the one that maximizes accuracy of the method. In addition to this, more
356 precise ranging sensors for height estimation will be studied in order to re-
357 duce the impact of mismatch measurements on the algorithm performance.
358 Furthermore, methods to overcome effects of tilting and rotation angles will
359 be studied and proposed.

360 Acknowledgments

361 Portion of this work was presented at the conference CSNDSP in 2016,
362 paper “A range free localization method for overlapped optical attocells using
363 neighbor’s information” [20].The authors acknowledge the financial support
364 of Beca Doctorado Nacional 2016 CONICYT (PFCHA) 21161397, STIC Am
365 Sud 19-STIC-08 and Fondef Proyecto IT17M10012.

366 References

- 367 [1] C. Van Slyke, Information communication technologies : concepts,
368 methodologies, tools and applications, Information Science Reference,
369 New York, USA, 2008.
- 370 [2] BusinessWire, Retail Indoor Location Market Breaks US\$10 Billion in
371 2020, Says ABI Research, 2015.
- 372 [3] H. Liu, H. Darabi, P. Banerjee, J. Liu, Survey of wireless indoor posi-
373 tioning techniques and systems, IEEE Transactions on Systems, Man
374 and Cybernetics Part C: Applications and Reviews 37 (2007) 1067–1080.
- 375 [4] R. Mautz, Indoor Positioning Technologies, 2012.
- 376 [5] P. Krishnamurthy, Technologies for Positioning in Indoor Areas, in:
377 Indoor Wayfinding and Navigation, 2015, pp. 35–51.

- 378 [6] P. H. Pathak, X. Feng, P. Hu, P. Mohapatra, Visible Light Communi-
379 cation, Networking, and Sensing: A Survey, Potential and Challenges,
380 IEEE Communications Surveys and Tutorials 17 (2015) 2047–2077.
- 381 [7] T.-H. Do, M. Yoo, An in-Depth Survey of Visible Light Communication
382 Based Positioning Systems, Sensors 16 (2016) 678.
- 383 [8] P. Huynh, M. Yoo, VLC-Based Positioning System for an Indoor Envi-
384 ronment Using an Image Sensor and an Accelerometer Sensor., Sensors
385 (Basel, Switzerland) 16 (2016) 783–799.
- 386 [9] Y. Zhuang, L. Hua, L. Qi, J. Yang, P. Cao, Y. Cao, Y. Wu, J. Thompson,
387 H. Haas, A Survey of Positioning Systems Using Visible LED Lights,
388 IEEE Communications Surveys and Tutorials 1 (2018) 1963 – 1988.
- 389 [10] D. Karunatilaka, F. Zafar, V. Kalavally, R. Parthiban, LED Based
390 Indoor Visible Light Communications: State of the Art, IEEE Commu-
391 nications Surveys & Tutorials 17 (2015) 1649–1678.
- 392 [11] X. Huang, J. Li, N. Chi, Y. Wang, Y. Wang, C. Yang, Experimental
393 demonstration for high speed integrated visible light communication and
394 multimode fiber communication system, IET Optoelectronics 9 (2015)
395 207–210.
- 396 [12] A. Yassin, Y. Nasser, M. Awad, A. Al-Dubai, R. Liu, C. Yuen,
397 R. Raulefs, E. Aboutanios, Recent Advances in Indoor Localization:
398 A Survey on Theoretical Approaches and Applications, IEEE Commu-
399 nications Surveys & Tutorials 19 (2017) 1327–1346.
- 400 [13] N. U. Hassan, A. Naeem, M. A. Pasha, T. Jadoon, C. Yuen, Indoor
401 Positioning Using Visible LED Lights, ACM Computing Surveys 48
402 (2015) 1–32.
- 403 [14] R. Hou, Y. Chen, J. Wu, H. Zhang, A Brief Survey of Optical Wireless
404 Communication, in: 13th Australasian Symposium on Parallel and Dis-
405 tributed Computing (AusPDC 2015), volume 163, Sydney, Australia,
406 pp. 41–50.
- 407 [15] K. Yan, H. Zhou, H. Xiao, X. Zhang, Current status of indoor posi-
408 tioning system based on visible light, in: 2015 15th International Con-
409 ference on Control, Automation and Systems (ICCAS), IEEE, Busan,
410 South Korea, 2015, pp. 565–569.

- 411 [16] J. Armstrong, Y. Sekercioglu, A. Neild, Visible light positioning: a
412 roadmap for international standardization, *IEEE Communications Mag-*
413 *azine* 51 (2013) 68–73.
- 414 [17] Y. Liu, Z. Yang, X. Wang, L. Jian, Location, localization, and localiz-
415 ability : location-awareness technology for wireless networks, volume 25,
416 Springer, New York, USA, 2010.
- 417 [18] G. Shi, Ge Shi, Yong Li, Li Xi, Baitao Zang, A Robust Method for
418 Indoor Localization Based on Visible Light Communication, in: 2016
419 2nd IEEE International Conference on Computer and Communications
420 (ICCC), IEEE, Chengdu, China, 2016, pp. 2154–2158.
- 421 [19] S. Subedi, G.-R. Kwon, Seokjoo Shin, Suk-seung Hwang, Jae-Young
422 Pyun, Beacon based indoor positioning system using weighted cen-
423 troid localization approach, in: 2016 Eighth International Conference
424 on Ubiquitous and Future Networks (ICUFN), IEEE, 2016, pp. 1016–
425 1019.
- 426 [20] F. Seguel, I. Soto, N. Krommenacker, P. Charpentier, P. Adasme, A
427 range free localization method for overlapped optical attocells using
428 neighbor’s information, in: 2018 11th International Symposium on Com-
429 munication Systems, Networks & Digital Signal Processing (CSNDSP),
430 IEEE, 2018, pp. 1–6.
- 431 [21] F. Seguel, N. Krommenacker, P. Charpentier, V. Bombardier, I. Soto,
432 Convex Polygon Positioning for Homogeneous Optical Wireless Net-
433 works, in: 2018 International Conference on Indoor Positioning and
434 Indoor Navigation (IPIN), IEEE, 2018, pp. 1–7.
- 435 [22] F. Seguel, N. Krommenacker, P. Charpentier, I. Soto, Visible light po-
436 sitioning based on architecture information: method and performance,
437 *IET Communications* 13 (2019) 848–856.
- 438 [23] T. Komine, M. Nakagawa, Fundamental analysis for visible-light com-
439 munication system using LED lights, *IEEE Transactions on Consumer*
440 *Electronics* 50 (2004) 100–107.
- 441 [24] P. Lou, H. Zhang, X. Zhang, M. Yao, Z. Xu, Fundamental analysis
442 for indoor visible light positioning system, 2012 1st IEEE International

- 443 Conference on Communications in China Workshops, ICCC 2012 (2012)
444 59–63.
- 445 [25] A. K. Gupta, A. Chockalingam, Performance of MIMO Modulation
446 Schemes With Imaging Receivers in Visible Light Communication, *Journal of Lightwave Technology* 36 (2018) 1912–1927.
447
- 448 [26] Elecfreaks, HC-SR04 User Guide (2018).
- 449 [27] ST Microelectronics, VL53L1X Datasheet (2018).
- 450 [28] G. Prince, T. Little, Two-Phase Framework for Indoor Positioning Sys-
451 tems Using Visible Light, *Sensors* 18 (2018) 1917.
- 452 [29] M. Pasha, C. Yuen, N. Hassan, U. Nadeem, Indoor positioning system
453 designs using visible LED lights: performance comparison of TDM and
454 FDM protocols, *Electronics Letters* 51 (2015) 72–74.
- 455 [30] L. Doherty, K. Pister, L. El Ghaoui, Convex position estimation in
456 wireless sensor networks, in: *Proceedings IEEE INFOCOM 2001. Conference on Computer Communications. Twentieth Annual Joint Conference of the IEEE Computer and Communications Society (Cat. No.01CH37213)*, volume 3, IEEE, Anchorage, USA, 2001, pp. 1655–1663.
457
458
459
460
- 461 [31] S. P. Boyd, L. Vandenberghe, *Convex optimization*, Cambridge University Press, New York, USA, 2004.
462
- 463 [32] M. C. Grant, S. P. Boyd, Graph Implementations for Nonsmooth Convex
464 Programs, in: B. Vincent, B. Stephen, K. Hidenori (Eds.), *Recent Advances in Learning and Control*, Springer London, London, UK, 2008, pp. 95–110.
465
466
467